UNIVERSITYOF BIRMINGHAM

Research at Birmingham

Encapsulation stability of duplex emulsions prepared with SPG cross-flow membrane, SPG rotating membrane and rotor-stator techniques—A comparison

Pawlik, Aleksandra; Norton, Ian

[Link to publication on Research at Birmingham portal](#)

ELSEVIER

Encapsulation stability of duplex emulsions prepared with SPG cross-flow membrane, SPG rotating membrane and rotor-stator techniques—A comparison

Aleksandra K. Pawlik*, Ian T. Norton

Centre for Formulation Engineering, Department of Chemical Engineering, University of Birmingham, Edgbaston, Birmingham, B15 2TT, UK

ABSTRACT

Food grade duplex $W_1/O/W_2$ emulsions were prepared using three different techniques: SPG cross-flow membrane, SPG rotating membrane and high-shear mixer. The primary W_1/O emulsion had sodium chloride encapsulated in the inner aqueous droplets as a marker compound. Duplex emulsion droplet size and salt encapsulation were both investigated by modifying the emulsification conditions inherent for each technique; cross-flow velocity (CFV) and trans-membrane pressure (TMP) for the cross-flow membrane, rotational velocity (RV) and TMP for the rotating membrane, and mixing time for the high-shear mixer.

Emulsion droplet size was shown to increase with TMP and to decrease with both CFV and RV. Minimum droplet size obtained ($\sim 12\,\mu m$) was similar for all three emulsifying techniques, which suggests that at high shear stresses, the minimum droplet size is determined primarily by the decrease in the interfacial tension.

It was also shown that the amount of salt released during storage depends on the emulsification technique (8–20% for the cross-flow membrane, $\sim 13\%$ for the high-shear mixer and $\sim 8\%$ for the rotating membrane). The differences in salt release were explained in terms of emulsions droplet size and interfacial properties of adsorbed surfactant molecules. The unexpected high amount of salt released by duplex emulsions produced by the cross-flow membrane was associated with the magnitude and duration of shear forces, which act on duplex droplets during semi-batch emulsification.

© 2012 Elsevier B.V. All rights reserved.

1. Introduction

Duplex emulsions (double or multiple emulsions) are emulsions of a complex microstructure where the dispersed droplets contain even smaller droplets inside. The application of duplex emulsions has long been appreciated by pharmaceutical, food, cosmetic and separation sciences. For example, in food products, the use of duplex water-in-oil-in-water ($W_1/O/W_2$) emulsions allows for substantial fat reduction as the dispersed phase is made up of water contained in the internal aqueous phase. Therefore, fat can be reduced without a change of droplet size or phase content. These systems can be also used to encapsulate and protect bioactive components, whilst delivering them to specific sites within the human body (e.g., mouth, stomach, small intestine etc.) [1]. However, the successful use of duplex emulsions as structured food products has been hindered by instabilities in their structure [2].

Duplex emulsions are normally prepared in a two-step emulsification process. The primary emulsion is typically prepared under intense homogenisation conditions in order to convert two immiscible fluids into an emulsion, or to reduce the size of a pre-existing emulsion. In the food industry this process is usually carried out using mechanical devices (e.g., high speed blenders, high-pressure homogenisers, colloid mills), where the dispersed phase is broken up by turbulent shear stresses. The secondary emulsification step is usually carried out under mild conditions in order to avoid the rupture of the internal droplets [3,4]. Using membranes for the secondary emulsification step offers the possibility of (i) good control over droplet size and droplet size distributions, (ii) low energy consumption (important for temperature sensitive components and economic savings [5]), and most importantly (iii) mildness of the process.

Depending on the required characteristics of the final emulsion, different types of membranes can be used: Shirasu Porous Glass (SPG) membrane, polymer, ceramic and metal membranes [6]. These membranes are characterised by various surface properties, mean pore size and effective membrane areas. Amongst them, SPG membranes have the advantage of wide availability, narrow pore size distributions (widely considered to be the most critical factor for the production of monodisperse emulsions [7,8]), wide range of available pore sizes (0.05–30 µm), high porosity (50–60% [6]) and excellent thermal stability for practical use [9].

The need for a mild secondary emulsification step in the processing of duplex emulsions makes membrane emulsification particularly desirable, as it is claimed [10] to enable high encapsulation yields of the internal droplets in the final product. Even though much work has been done [11–16], investigation of the influence of membrane emulsification parameters on the droplet size and droplet size distribution in $W_1/O/W_2$ duplex emulsions, and encapsulation and marker release from these, remains scarcely explored [13,15,17]. Okochi and Nakano [17] compared the encapsulation of water-soluble pharmaceutical drugs in $W_1/O/W_2$ emulsions prepared with the SPG membrane (secondary emulsification step) and a stirring method (both emulsification steps). They found that the encapsulation was higher for membrane emulsification and this was mainly associated with more homogenous particles and reduced surface area due to the absence of small droplets.

Rotating membrane emulsification is a relatively new technique and there are only a small number of publications on this subject [5,18,19]. All the reported research focuses on stainless steel rotating membranes, which were successfully used in the manufacture of simple (and mostly coarse [18,19]) O/W emulsions where RV, TMP, width of the gap, membrane pore geometry and emulsion composition were analysed in relation to the microstructure of the emulsion.

Our work aims to understand the effects of RV and TMP on the encapsulation properties and microstructure of duplex $W_1/O/W_2$ emulsions manufactured using the SPG rotating membrane. In this study we also investigate whether $W_1/O/W_2$ duplex emulsions prepared with the cross-flow and the rotating membrane have better quality than duplex emulsions prepared in the high-shear process. It will be shown that due to vigorous processing inside the cross-flow membrane module, emulsions prepared with this technique released similar amount of salt to emulsions prepared with the high-shear mixer. It will be also demonstrated that in both membrane techniques, the duplex droplet size reduces with applied CFV or RV, and increases with TMP.

2. Materials and methods

2.1. Materials

The oil soluble emulsifier polyglycerol polyricinoleate (PGPR) Admul WOL 1408 ($HLB = 1.5 \pm 0.5$) was kindly provided by Kerry Bio-Science (The Netherlands). Tween 20 ($HLB = 16.7$), glucose, NaCl were purchased from Sigma Aldrich (UK). The sunflower oil used was commercially available. All experiments were performed using distilled water (conductivity 1.3–1.5 μS cm^{-1}). All materials were used without further purification or modification of their properties.

2.2. Preparation of the primary W_1/O emulsion

Thirty percent water-in-oil emulsions (W_1/O) were prepared in a high-shear mixer (Silverson SL2T) at 10,000 rpm for 10 min after the addition of the water phase; 300 g batch size mixed in a 500 mL glass beaker. First, oil soluble emulsifier was added into the oil phase and stirred for 5 min. Then while homogenising, the water phase with 0.28 M NaCl (as a marker compound [20]) was added drop-wise to the oil mixture containing the emulsifier (PGPR, 4 w/w%). The system was cooled during the homogenisation step to 20–30 °C by means of an ice bath. After preparation, emulsions were analysed for droplet size and then stored at ~5 °C. The average droplet diameter of the W_1/O emulsion was 200 nm, and did not change over the storage period of 18 weeks [21]. All compositions were prepared by weight per cent.

2.3. Preparation of $W_1/O/W_2$ duplex emulsions

2.3.1. High-shear mixer

Glucose (used to balance the osmotic pressures between the two aqueous phases) and Tween 20 (2 w/w%) were mixed with water for 5 min prior to use. The primary W_1/O emulsion was placed on the top of the water phase and homogenised at 10,000 rpm for 2, 5 and 10 min using a Silverson mixer (model L4RT with 21 and 21.5 mm impeller and screen diameter, respectively); 150 g batch size in a 250 mL glass beaker. All duplex emulsions (with 30% of W_1/O in 70% of W_2) were analysed immediately after preparation and then stored at ~5 °C.

2.3.2. Cross-flow membrane emulsification

Shirasu Porous Glass (SPG) hydrophilic membrane with a pore size of 3.9 μm was purchased from SPG Technology Co. (Japan). The SPG membrane is tubular, 10 mm in outer diameter, 250 mm in length, giving an approximate surface area of 78 cm^2. Prior to emulsification, the membrane was pre-wetted with distilled water and treated in an ultrasonic bath for 3 h to remove residual air, and enable micropores to be filled with the continuous phase. After emulsification, the membrane was cleaned with a soap solution in the ultrasonic bath (until the solution was clean), and then sonicated again with ethanol for 3 h. After rinsing with distilled water, the membrane was dried at 60 °C for 12 h, and then soaked in the continuous phase while sonicated. If this was not sufficient to fully clean the membrane, then it was heated in a
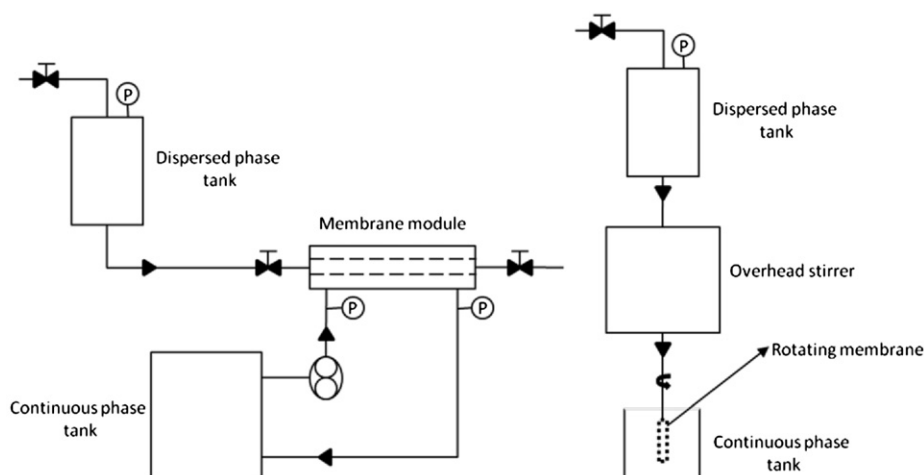

Fig. 1. Schematic diagram of cross-flow membrane (left) and rotating membrane (right) set-up.

muffle furnace at 500 °C for 24 h, to burn all the residual oils [22]. After the heat treatment, the membrane was soaked in 2 M HCl at 70 °C for 2 h, to restore surface hydrophilicity, and finally rinsed with distilled water.

The cross-flow membrane emulsification apparatus is schematically presented in Fig. 1 (left). The continuous water phase (W_2) containing Tween 20 and glucose was pumped through the apparatus (i.e., the annulus between the membrane and the metal module housing it) by a gear pump. The reason behind this rather unconventional direction of the disperse phase flow through the membrane (i.e., inside-out), was to minimise droplets collisions (hence coalescence) in the mainstream of the continuous phase, but also ensure laminar flow conditions, as the effective gap between the membrane and the module enclosing it was small (2 mm). Three different pressures exerted by the continuous phase on the membrane surface (10, 30 and 50 kPa) were chosen. The dispersed phase, in this case—W_1/O emulsion, pressurised in the vessel, was forced through the membrane pores by compressed air at TMPs of 20, 40 and 80 kPa. The TMP was calculated as the difference between the dispersed phase pressure and the pressure exerted on the membrane by the continuous phase. For further analysis, CFVs were calculated from the volumetric flow rates of the emulsion in the membrane module, for each continuous phase pressure (Table 1). As emulsification is a semi-batch process, the dispersed phase volume fraction increases with emulsification progression. This leads to an increase in the overall viscosity of the emulsion, thus an increase in the pressure exerted by the continuous phase on the membrane, and a subsequent drop in

the effective TMP. To maintain constant TMP we opted for practical reasons, to manually reduce the CFV by controlling the pump speed. Due to the increasing viscosity of the produced emulsion, two situations have been considered for calculations: (i) $T_{0\%}$ when the dispersed phase volume is 0% (start of the emulsification process), and (ii) $T_{30\%}$ when the dispersed phase volume is 30% (end of the emulsification process). To simplify the way the CFV is referenced in further text, an average of $T_{0\%}$ and $T_{30\%}$ was calculated and consequently used for the respective continuous phase pressure (Table 1).

The batch size of 150 g for cross-flow membrane emulsification was identical to the high-shear emulsification; 30% of which was the dispersed phase (W_1/O). The desired dispersed volume fraction was assessed by weighing the duplex emulsion throughout the emulsification process, and terminating the disperse phase flow at a required weight. Silicone tubing with a total length of 118 cm was used. Each experiment was repeated three times at the temperature of 21 ± 1 °C.

2.3.3. Rotating membrane emulsification

A schematic diagram of the rotating membrane set up is shown in Fig. 1 (right). A 5 cm long, tubular, hydrophilic SPG membrane with 2.8 μm mean pore diameter was mounted on a threaded ferrule, which was then attached to an IKA Eurostar Digital overhead stirrer. The speed of membrane rotation was set at 300, 600, 900 and 1200 rpm. The dispersed phase (W_1/O) was pressurised through the membrane pores by compressed air at the TMP of 40, 60, 80 and 100 kPa. The batch size, dispersed phase volume fraction, membrane preparation, emulsification procedure (number of repetitions and storage) and the cleaning process (without heat treatment), were identical to the cross-flow membrane emulsification technique.

2.4. Shear calculations

In order to compare the three emulsification techniques described above, relative shear stresses that the emulsion droplets are subjected to during each process were calculated. The analysis is given in Table 2.

Table 1
Relationship between cross-flow velocity and continuous phase pressure; $T_{0\%}$ is for 0% dispersed phase volume system and $T_{30\%}$ is for 30% dispersed phase volume system.

Continuous phase pressure [kPa]	Cross-flow velocity [m s^{-1}]		
	$T_{0\%}$	$T_{30\%}$	Average
10	0.16	0.06	0.11
30	0.23	0.11	0.17
50	0.29	0.15	0.22

Table 2
Shear stress and shear rate values for all three emulsification systems.

			Shear rate [s^{-1}]	Shear stress [Pa]
High-shear mixer			21,980	145
Cross-flow membrane	**Cross-flow velocity**			**Wall shear stress [Pa]**
	0.11 m s^{-1}	$T_{0\%}$	317	0.26
		$T_{30\%}$	116	1.61
	0.17 m s^{-1}	$T_{0\%}$	455	0.38
		$T_{30\%}$	212	2.94
	0.22 m s^{-1}	$T_{0\%}$	576	0.48
		$T_{30\%}$	295	4.10
Rotating membrane	**Rotational velocity**			**Shear stress [Pa]**
	300 rpm	$T_{0\%} R_i$	65	0.054
		$T_{0\%} R_o$	2.4	0.002
		$T_{30\%} R_i$	65	0.332
		$T_{30\%} R_o$	2.4	0.012
	600 rpm	$T_{0\%} R_i$	130	0.108
		$T_{0\%} R_o$	4.8	0.004
		$T_{30\%} R_i$	130	0.664
		$T_{30\%} R_o$	4.8	0.024
	900 rpm	$T_{0\%} R_i$	196	0.162
		$T_{0\%} R_o$	7.2	0.006
		$T_{30\%} R_i$	196	0.997
		$T_{30\%} R_o$	7.2	0.037
	1200 rpm	$T_{0\%} R_i$	261	0.217
		$T_{0\%} R_o$	9.6	0.008
		$T_{30\%} R_i$	261	1.329
		$T_{30\%} R_o$	9.6	0.049

For the high-shear mixer, the shear rate was calculated from the gap between rotor and stator where the highest energy dissipation occurs [23]:

$$\gamma = \frac{\pi ND}{\delta} \tag{1}$$

where γ is the shear rate at the gap [s^{-1}], N is the agitation speed [s^{-1}], D is the diameter of an impeller [m], and δ is the gap between the impeller and the screen [m]. The shear stress τ [Pa] was obtained from the following relationship with viscosity μ [Pa s] for Newtonian fluids:

$$\tau = \mu\gamma \tag{2}$$

For the cross-flow membrane, γ was calculated from a wall shear stress (τ_w) and Eq. (2) for each CFV, as shown in Table 2. Due to the batch nature of the emulsification process, as explained in Section 2.3.2, calculations were performed for both limiting conditions: at the beginning ($T_{0\%}$) and at the end ($T_{30\%}$) of the emulsification process.

$$\tau_w = 0.5 f_F \rho v^2 \tag{3}$$

$$\text{for } Re < 2000 \quad f_F = \frac{16}{Re} \tag{4}$$

$$Re = \frac{\rho v D_h}{\mu} \tag{5}$$

where f_F the Fanning friction factor, ρ is the fluid density [kg m^{-3}], v is the CFV [m s^{-1}], Re is the Reynolds number, D_h is the hydraulic diameter of the membrane annulus [m] and μ is the dynamic viscosity [Pa s].

For the rotating membrane, shear rate was estimated in the same way as for the cross-flow emulsification, at $T_{0\%}$ and $T_{30\%}$ and all RVs. It was based on a Taylor–Couette model of concentric cylinders with a wide gap between them. Due to the width of the gap, the simple shear between the cylinders is disturbed by the secondary flow induced by the formation of Taylor vortices. Shear rate at the surface of the membrane (at R_i) is expressed by:

$$\gamma = \frac{2\omega a^2}{a^2 - 1} \tag{6}$$

Shear rate at the wall of an emulsification beaker (at R_o) can be written as:

$$\gamma_0 = \frac{2\omega}{a^2 - 1} \tag{7}$$

where $a = R_o/R_i$ where ω is the RV [s^{-1}], R_o is the radius of the beaker (external cylinder) and R_i is the radius of the rotating membrane (internal cylinder).

2.5. Droplet size

Droplet sizes of duplex emulsions were analysed using a Malvern Mastersizer®2000 (UK) with a Hydro SM manual small volume sample dispersion unit attached. Measurements were performed in distilled water as described in our previous work [21]. The average droplet diameter was expressed as a Sauter diameter, $D_{3,2}$.

2.6. Interfacial tension

The interfacial tension of surfactant solutions was measured using a pendant drop method on an EASYDROP Contact Angle Measuring System from Krüss GmbH, Hamburg (Germany). In this method, a droplet of surfactant solution was formed at the tip of a syringe needle, immersed in a cuvette containing sunflower oil with an oil-soluble surfactant (PGPR). By analysing the shape

of the drop using a suitable mathematical model, the interfacial tension was obtained [24].

2.7. Conductivity

The conductivity of duplex emulsions during emulsification (or immediately after) and storage, was measured by a direct current conductivity meter S30 SevenEasy™ fitted with an InLab®710 platinum 4—plate electrode (Mettler Toledo, UK), which has a measurement range of 0.01–500 mS cm^{-1}. The conductivity meter was connected to a PC equipped with a RS323 DataLogger and measurements recorded every 1.25 s.

A model (Eq. (8)) developed by Meredith and Tobias [25] for describing the conductivity changes of an emulsion (k_e), was used to fit the data obtained from experiments and calibrations [21]. According to this method, conductivity of an emulsion is related to the volume fraction of the dispersed phase and the conductivity of the continuous phase. If the conductivity of the dispersed phase (k_d) is much lower than the conductivity of the continuous phase (k_c), the conductivity of an emulsion can be described by:

$$k_e = 8 k_c \frac{(2-\phi)(1-\phi)}{(4+\phi)(4-\phi)} \tag{8}$$

where k_e is the conductivity of the bulk emulsion and Φ is the dispersed phase volume fraction.

The conductivity of a duplex emulsion's external water phase was calculated using Eq. (8) and the measured conductivity of the $W_1/O/W_2$ emulsion. From the linear calibration curve for the conductivity of glucose and Tween 20 solutions with varying NaCl concentration, the amount of salt released from the internal to external water phase was determined. The encapsulation was then expressed as a percentage of salt still retained (encapsulated) in the internal water phase:

$$\text{Encapsulation} = \frac{100x(M_t - M_r)}{M_t} \tag{9}$$

where M_t is the total original mass of salt present in the internal water phase and M_r is the mass of NaCl that migrated to the external water phase.

3. Results and discussion

3.1. Process effect on duplex emulsion droplet size

High-shear mixer, cross-flow membrane and rotating membrane emulsification techniques were employed to produce duplex $W_1/O/W_2$ emulsions. The effect of emulsification parameters on duplex emulsion droplet size was investigated. All emulsions were examined for droplet size immediately after preparation and then in regular time intervals during storage.

3.1.1. High-shear mixer
When duplex emulsions were prepared using the high-shear mixer, different mixing times were applied in order to find the optimal emulsion droplet size. Droplet size distribution curves of emulsions homogenised for 2, 5 and 10 min are given in Fig. 2. It can be seen that there is no appreciable difference between them, i.e., comparable average droplet sizes for all emulsions (13.6 ± 0.6 μm) and similar size distributions. This shows that the droplet size obtained after 2 min of high-shear mixing cannot be further reduced by longer application of shear (i.e., 5 and 10 min). These data suggest that the droplet size of $\sim$14 μm is the minimum droplet size that can be obtained for this specific formulation under the investigated emulsification conditions.

3.1.2. Cross-flow membrane emulsification
In cross-flow membrane emulsification, the effects of TMP and CFV were investigated in relation to the duplex emulsion droplet size. Changes in emulsion droplet size with CFV and TMP are shown in Fig. 3. On the Y-axis of the graph, mean droplet size of all emulsions (mixed for 2, 5 and 10 min) made with the high-shear mixer ($\sim$14 μm) has been plotted as a reference.

As shown in Fig. 3, the average droplet size decreases as CFV increases for a given TMP. For example, at 40 kPa TMP the droplet sizes are $\sim$35 μm for
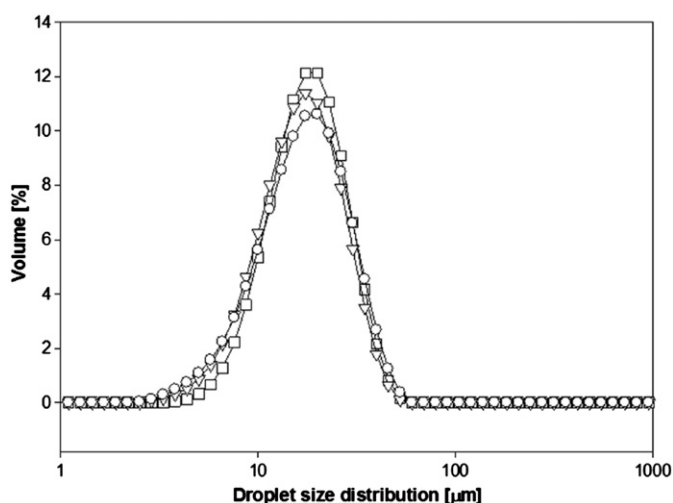
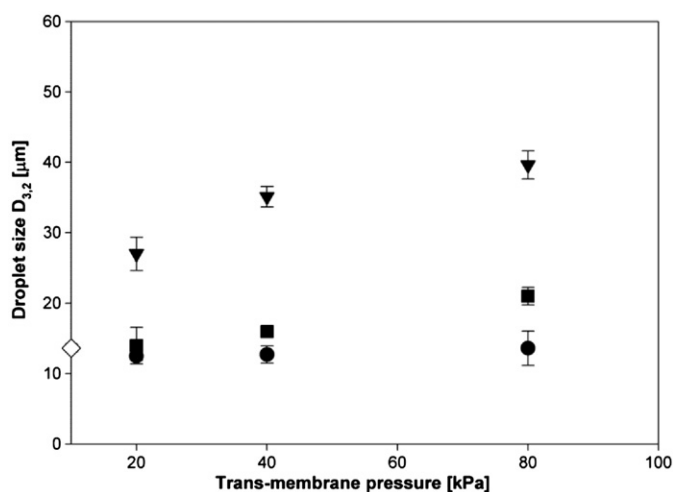**Fig. 2.** Droplet size distributions of duplex emulsions homogenised in the high-shear mixer at 10,000 rpm for ($\square$) 2 min, ($\triangledown$) 5 min and ($\circ$) 10 min.

Fig. 3. Cross-flow membrane; effect of TMP and CFV: ($\blacktriangledown$) 0.11 m s^{-1}, ($\blacksquare$) 0.17 m s^{-1}, ($\bullet$) 0.22 m s^{-1} on duplex emulsion droplet size ($D_{3,2}$). Note: on the Y-axis ($\diamond$ is the mean droplet size for emulsions made with the high-shear mixer.

0.11 m s^{-1}, ~16 μm for 0.17 m s^{-1} and ~13 μm for 0.22 m s^{-1} CFV. This observation is widely reported in the literature for single [26] and duplex emulsions [11] produced by membrane emulsification. A possible explanation for such behaviour comes from the fact that the flow of the continuous phase generates hydrodynamic drag, which is a major driving force for the detachment of droplets from membrane pores. Consequently, with increasing CFV, smaller droplets are formed due to earlier detachment, as a result of larger drag forces.

Fig. 3 also shows that at high CFV (0.22 m s^{-1}): (i) the smallest emulsion droplet sizes are obtained and, (ii) the TMP has no (or only little) effect on the droplet size (e.g., 12.5 ± 0.6 μm at 20 kPa, 12.7 ± 1.2 μm at 40 kPa and 13.6 2.4 μm at 80 kPa TMP). This can be explained by a force balance model. In cross-flow membrane emulsification, droplets grow at pores and detach at a certain volume, which is determined by the balance of forces acting on the droplet [27]. Based on their order of magnitude, the main forces are: the drag force and the interfacial tension force. According to Peng and Williams [26], the final (experimental) volume of the droplet V_d [m^3] is a sum of (i) theoretically calculated volume (V_{calc}) that depends on the balance of forces acting on the droplet during its inflation, and (ii) the volume added to the droplet during its detachment; which in turn is determined by the flow rate of the dispersed phase Q [m^3 s^{-1}] and the detachment time t [s]:

$$V_d = V_{calc} + Qt \tag{10}$$

It could be assumed, that at high CFV (i.e., 0.22 m s^{-1}), the time for the droplet detachment may be relatively small [7]. This makes Qt insignificant and droplets break off the pore tip after reaching the *droplet growth* volume. V_g is determined

by the decrease in the interfacial tension between the two phases (down to ~1 mN m^{-1}) and the applied shear at the surface of the membrane.

The situation is different when the CFV is smaller (i.e., 0.11 and 0.17 m s^{-1}). With decreasing CFV, the effect of the dispersed phase flow on the droplet diameter is more significant. The diameter of droplets increases with TMP; from ~27 μm at 20 kPa TMP to ~40 μm at 80 kPa (CFV=0.11 m s^{-1}). This finding is supported by previous research by Joscelyne and Trägårdh [8], who reported that the largest change in droplet size occurs at small wall shear stresses.

There are several possible reasons that alone, or more likely in combination, are responsible for the formation of larger droplets with increasing TMP. First, according to Darcy's law, the flow through the pores should increase with TMP in a linear way [28]. As a result, more liquid is pumped into the drop, increasing its volume before detachment. Second, the increase in droplet diameter may result from the mechanism of droplet formation, which changes with increasing trans-membrane fluxes. At low TMP, droplets are created via *a dripping mechanism* [29], where as soon as the droplet is formed at the pore tip, the hydrodynamic drag force of the continuous phase helps the droplet to break away from the membrane. On the contrary, at higher trans-membrane fluxes droplets are formed in *a continuous jetting regime* [26]. This increases the probability of droplet coalescence at the membrane surface [30], resulting in a larger average droplet diameter. Third, larger droplets at higher TMPs could also be as a result of more membrane pores being activated [31]. In this case, droplets formed at neighbouring pores are likely to come into contact and coalesce [32], encouraged by the direction of the flow of the continuous phase parallel to the membrane's surface. Lastly, it has been reported [31] that the rate of surfactant adsorption onto the newly formed interface has an effect on the droplet size. When TMP increases, the rate of interface formation is relatively quick, and possibly comparable with the rate of the interfacial tension decrease. Low surfactant coverage would lead to: (i) a larger interfacial tension thus larger forces opposing droplet detachment and (ii) droplet coalescence during formation and in the bulk emulsion (post-formation). As a consequence, larger droplets are produced [33].

In order to correlate the membrane pore size and the diameter of produced droplets, the ratio of d_{drop}/d_{pore} was calculated. Our data for the 3.9 μm cross-flow membrane gives values of 3–10, which fall within the range of reported values in literature [8,12,27,30] of 2–10.

3.1.3. Rotating membrane emulsification

In rotating membrane emulsification, TMP and RV were varied in order to understand their effect on duplex emulsion droplet size. In Fig. 4 changes in emulsion droplet size with TMP and RV are given. It is shown that at low RV (300 rpm), droplet size increases substantially with TMP. For example, emulsions produced at 40 kPa TMP have droplet sizes of ~20 μm, which increases to ~30 μm at 60 kPa, to ~35 μm at 80 kPa and finally to ~40 μm at 100 kPa. This progressive increase is probably due to the mechanisms of droplet formation described in Section 3.1.2, for small CFVs in the cross-flow membrane technique.

The smallest emulsion droplets were obtained at the highest RV (1200 rpm) and showed no significant dependence to TMP (e.g., 8.5 ± 1.7 μm at 40 kPa increased to 12.8 ± 1.5 μm at 100 kPa). This corresponds to a trend observed in droplet size data obtained for the cross-flow membrane (Fig. 3), and suggests that at high wall shear stresses, RV and CFV have a similar effect on duplex emulsion droplet size.

At intermediate RVs (600 and 900 rpm), emulsion droplet sizes are comparable over the range of applied TMPs. They initially increase from ~11 to ~22 μm
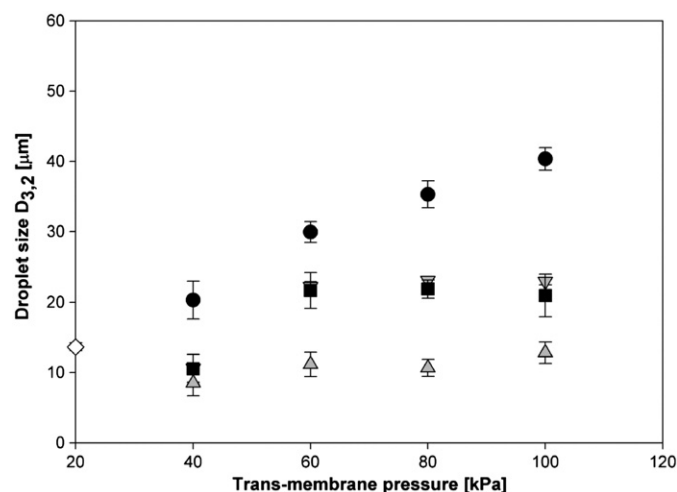
Fig. 4. Rotating membrane; effect of TMP and RV: ($\bullet$) 300 rpm, ($\blacktriangledown$) 600 rpm, ($\blacksquare$) 900 rpm, ($\blacktriangle$) 1200 rpm on duplex emulsion droplet size ($D_{3,2}$). Note: on the Y-axis ($\diamond$) is the mean droplet size for emulsions made with the high-shear mixer.

between 40 and 60 kPa and then remain constant at higher TMPs (~22 μm at 80 and 100 kPa). This suggests that at intermediate values of RV, a transition between the two mechanisms determining the emulsion droplet size occurs. This transition occurs between a low-shear mechanism (at 300 rpm), when TMP has a significant effect on droplet size, and a high-shear mechanism (at 1200 rpm), when TMP has very little influence on droplet size.

Fig. 4 also demonstrates that regardless of the TMP, increase in RV in general leads to a reduction in emulsion average droplet size. This is explained by the fact that increased rpm of the rotating membrane corresponds to higher shear stresses at the membrane wall (Table 2). This creates a larger detaching force and thus allows formation of smaller droplets.

The calculated d_{drop}/d_{pore} ratio for the 2.8 μm rotating membrane is between 3 and 14, which is slightly higher than the ratio for the cross-flow membrane. To the best of our knowledge, d_{drop}/d_{pore} ratios for the rotating SPG membranes have not been reported so far, which does not allow comparison with existing data. Comparison with the 3.9 μm cross-flow membrane (Table 2) shows that wall shear stresses for the investigated RVs of the rotating membrane are smaller (max. of ~1.3 Pa at 1200 rpm) than the wall shear stresses calculated for CFVs in cross-flow membrane emulsification (max. of ~4.1 Pa at 0.22 m s^{-1}). Therefore, it could be expected that the average droplet size would be larger for the rotating membrane, which leads to a larger d_{drop}/d_{pore} ratio. It was also observed that during the emulsification at 300 rpm, newly created droplets did not detach from the membrane immediately but rather built up at its surface. Due to a small centrifugal force a layer of droplets were formed at the membrane wall, and then slowly dispersed into the bulk upon further rotation of the membrane. The thickness of this layer was proportional to the TMP. This behaviour most probably leads to coalescence of droplets in the layer, resulting in bigger average droplet size and d_{drop}/d_{pore} ratio.

In summary, the minimum droplet size of emulsions obtained by all three emulsification techniques were similar; ~14 μm with the high-shear mixer (an average of all mixing times), ~13 μm with the cross-flow membrane technique (average at 0.22 m s^{-1} CFV), and ~11 m with the rotating membrane technique (average at 1200 rpm RV). However, shear forces created by these emulsifying techniques are markedly different (Table 2). All this suggests that when the maximum shear rate is applied in each of the emulsifying techniques, the minimum droplet size of the investigated duplex emulsions is determined by the interfacial tension force.

During long-term storage all produced emulsions increased in droplet size by an average of 1–2 μm. This was confirmed by microscopic analysis, which showed no significant change in the internal structure of duplex emulsions (i.e., the size of the primary water droplets, data not shown). Therefore, it was concluded that throughout the storage period there is no significant osmotic flow of water between the internal and the external emulsion phases.

3.2. Salt encapsulation during emulsification

The effect of emulsification parameters on the encapsulation of salt in the internal water phase (W$_1$) of duplex W$_1$/O/W$_2$ emulsions was investigated. The emulsion conductivity was measured during the emulsification process (for the high-shear mixer), or immediately after (for both membrane techniques).

3.2.1. High-shear mixer emulsification

The conductivity of duplex emulsions was measured throughout the high-shear emulsification and then for an additional 2 min after mixing had stopped. Fig. 5 shows the extent of salt release from the emulsion internal water phase during mixing for 2, 5 and 10 min. It can be seen that the three different mixing times resulted in significant differences in the salt release curves for the respective duplex emulsions. The emulsion mixed for 2 min released less salt (0.4%) than emulsions subjected to the shearing force for 5 and 10 min, which released considerably more salt (1.2% and 2.8%, respectively). This is probably due to a shear-induced breakage of the duplex emulsion structure and subsequent release of the internal water phase carrying the salt.

3.2.2. Cross-flow membrane emulsification

The effect of CFV and TMP on duplex emulsion stability during the emulsification process was investigated. Fig. 6a shows salt encapsulation in duplex emulsions measured directly after emulsification. It can be seen that for a given TMP, the encapsulation decreases with an increase in the velocity at which the continuous phase flows across the membrane. As shown in Table 2, the increase in CFV from 0.11 to 0.22 m s^{-1} causes an increase in the membrane wall shear stress from 1.61 to 4.10 Pa for the $T_{30\%}$ system, and consequently a rise in the overall shear stress acting on emulsion droplets in the membrane module and the tubing system. This may result in breakage of the shear-sensitive duplex droplets [34]. It has been suggested by van der Graaf et al., [16], that the external phase flow induces internal streaming in the duplex droplets, which increases the frequency of collisions (and thus coalescence) of the internal water droplets (W$_1$) with the outer water phase (W$_2$). In addition to emulsion damage induced by the fluid flow in the membrane module, breakage of duplex droplets may also occur in the gear pump, which is used to force the continuous phase through the
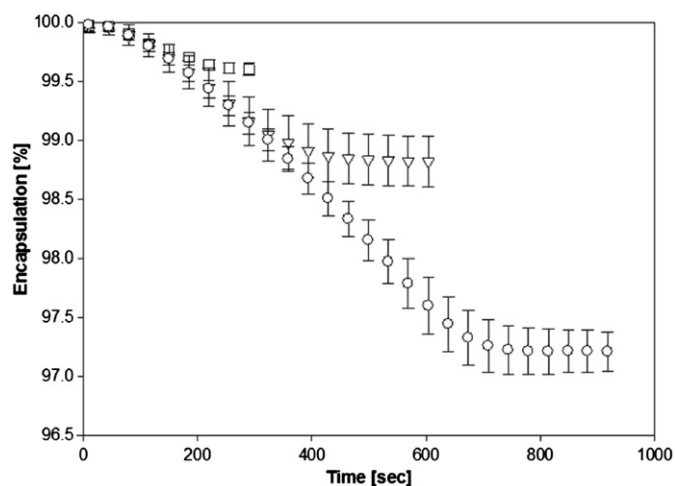
Fig. 5. Emulsification encapsulation of salt in duplex emulsions mixed with the high-shear mixer at 10,000 rpm for (□) 2 min, (▽) 5 min and (○) 10 min.
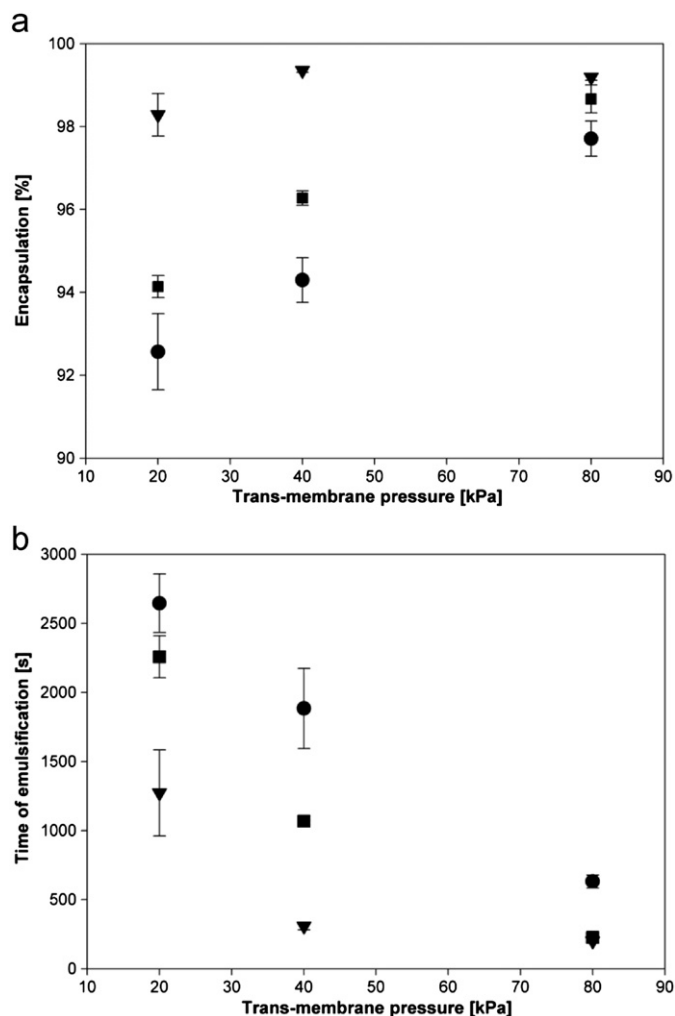
Fig. 6. Cross-flow membrane; (a) salt encapsulation in duplex emulsions measured just after emulsification and (b) time of batch emulsification. Effect of TMP and CFV: (▼) 0.11 m s^{-1}, (■) 0.17 m s^{-1} and (●) 0.22 m s^{-1}.

membrane module. The rotating pump gears transfer the emulsion with a very small mechanical clearance (typically in the order of 10 μm), to the discharge side of the pump. This may result in damage to the larger emulsion droplets during the pumping cycles and subsequent release of the internal water phase.

Fig. 6a also demonstrates that there is a strong effect of TMP on salt encapsulation. This is especially significant for 0.17 and 0.22 m s^{-1} CFV. Salt encapsulation at a given CFV increases with TMP and thus, according to Darcy's law, dispersed phase flux through the micropores. The increase in duplex encapsulation with TMP is most probably a consequence of the emulsification time; that is the time taken to produce a 30% dispersed phase volume $W_1/O/W_2$ emulsion at a given CFV and TMP. This time dependence is shown in Fig. 6b, where the emulsification time was plotted as a function of both CFV and TMP. It is shown that the emulsification time increases for smaller TMPs; for example at the CFV of 0.11 m s^{-1}, emulsification takes ∼200 s at 80 kPa, which increases to ∼300 s at 40 kPa and further to ∼1300 s at 20 kPa TMP. Due to the semi-batch emulsification procedure, duplex droplets produced at the beginning of the process continue to re-circulate within the continuous phase through the membrane module until the desired volume fraction of the dispersed phase is obtained. As a result, some droplets are exposed to the flow induced shear forces for longer, hence greater subsequent breakage of the duplex structure and release of the entrapped internal water phase with salt may occur.

The emulsification time dependence on TMP and CFV as shown in Fig. 6b, corresponds in trend and magnitude to the encapsulation dependence on TMP and CFV (Fig. 6a); namely salt release from duplex droplets increases at longer emulsification times. It also should be noted that for a given TMP, emulsification time increases with CFV. This is most probably due to fouling of the membrane, which may block the pores and/or reduce pore size, thus resisting flux of the dispersed phase.

3.2.3. Rotating membrane emulsification

Duplex $W_1/O/W_2$ emulsions produced with the rotating membrane were analysed for salt release directly after emulsification. Fig. 7 shows changes in the encapsulation of NaCl in duplex emulsions, depending on the applied TMP and RV. These data show that there are no significant differences in the release of salt within the investigated TMPs and RVs. Nevertheless, emulsions prepared using the rotating membrane released only small amounts of salt (up to 1.2%) during the emulsification process compared to the high-shear process (up to 2.8% for 10 min mixing) and the cross-flow membrane (up to 7.5% for 20 kPa TMP and 0.22 m s^{-1} CFV). It is suggested that emulsion droplet size, and thus interfacial area, has no effect on salt release during the emulsification process. This is due to the fact that: (i) in high-shear emulsification, the emulsions mixed for different times release different amounts of salt despite very similar droplet sizes, and (ii) the emulsions prepared with the rotating membrane released similar amounts of salt during emulsification, despite a relatively wide range of droplet sizes (between ∼8.5 and ∼40 μm). The reason for the observed variations in the encapsulation for emulsions produced using those three techniques could be the magnitude of shear forces that act on duplex droplets during the emulsification process.

All calculated shear rates and shear stresses for the three emulsification systems are given in Table 2. It shows that shear forces generated in the gap between the Silverson's rotor and stator are the highest (21,980 s^{-1}), followed by the cross-flow membrane (116–576 s^{-1}) and the rotating membrane (2.4–261 s^{-1}). In cross-flow membrane emulsification, shear stress increases with CFV and emulsification progress (from the $T_{0\%}$ to the $T_{30\%}$ system), as viscosity of the emulsion increases. In the emulsifying cylinder (beaker) of the rotating membrane, shear stress varies depending on the distance to the membrane and progress of emulsification. At the surface of the rotating membrane, shear stress is highest for the maximum rotational speed (i.e., 1200 rpm) and increases with
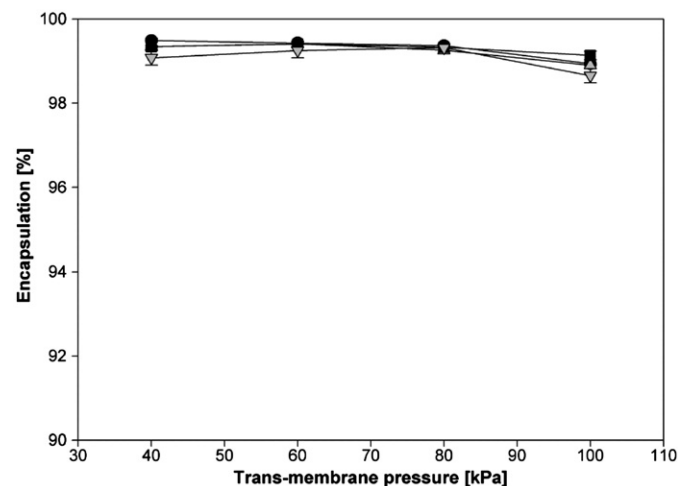
progress of emulsification (from 0.217 Pa at $T_{0\%}$ to 1.329 Pa at $T_{30\%}$, calculated for the surface of the rotating membrane R_i). Additionally, shear stress acting on duplex droplets in close proximity to the beaker wall is significantly smaller (0.008 Pa at R_o, $T_{0\%}$) than close to the membrane wall (0.217 Pa at R_i, $T_{0\%}$).

Since the release of internal droplets in duplex emulsions is dependent on the applied shear stress (due to droplet elongation [10]), minimum encapsulation would be expected in emulsions produced by the high-shear process. As given in Table 2 the shear stress acting on duplex droplets is much higher for the high-shear mixer than for the two membrane methods. However, the observed salt encapsulation in emulsions produced using the cross-flow membrane is similar or even lower (e.g., for 0.22 m s^{-1} CFV) than in emulsions made using the high-shear mixer. It is therefore likely, that the external phase flow in batch cross-flow emulsification, and the use of the gear pump, induce destructive shear forces in the system. This will cause duplex droplet damage and a decrease in emulsion quality.

3.3. Salt encapsulation on storage

All duplex emulsions were examined for salt release over the storage period of up to 60 day (for high-shear emulsification and the rotating membrane) and up to 70 day (for the cross-flow membrane).

3.3.1. High-shear mixer emulsification

Fig. 8 shows salt release profiles for emulsions prepared by mixing at 10,000 rpm for 2, 5 and 10 min. It can be seen that salt release over the storage period was the same for all three mixing times (∼12.6% loss of salt). This is contrary to the encapsulation measured directly after emulsification, when the release of salt varied significantly between emulsions with different mixing times (Fig. 5). These findings show that in this case, long-term salt release from duplex emulsions is not determined by the time droplets are subjected to shearing forces, but rather by the composition of both water phases and the chemical potential gradient between them. Furthermore, any possible damage that is done to the duplex structures during high-shear mixing does not influence long-term storage stability. An additional explanation for the similar release rates for the three emulsions may come from the fact that all emulsions have similar droplet sizes (∼14 μm), and thus comparable diffusion distances and surface areas available for molecular transport.

The overall rate of salt release is relatively low and similar to that reported for MgCl$_2$ [35]. We have shown in our previous work [21], that the release of salt is driven by the chemical potential difference rather that unbalanced osmotic pressures. During initial days of storage, the transport of salt across the oil phase is high due to a large gradient of electrolyte concentration in both water phases. Later, the rate of release slows down, as the concentration of NaCl in the two water phases tends to equilibrate. In the same work, we have shown that the addition of salt alters the interfacial properties of the adsorbed surfactant, increasing its visco-elastic properties. This was associated with formation of "solid-like" domains at the interface, which by increasing molecular interactions in the adsorbed film may create a mechanical barrier against coalescence and molecular transport. Additionally, all samples were kept at low temperature (5 ± 2 °C), which combined with a relatively high viscosity of the primary W_1/O emulsion (∼0.2 Pa s, measured at 25 °C and a shear rate of 11 s^{-1}) result in slow, yet sustained salt release.

Fig. 7. Rotating membrane; salt encapsulation in duplex emulsions measured just after emulsification. Effect of TMP and RV: (●) 300 rpm, (▲) 600 rpm, (■) 900 rpm, (▼) 1200 rpm.
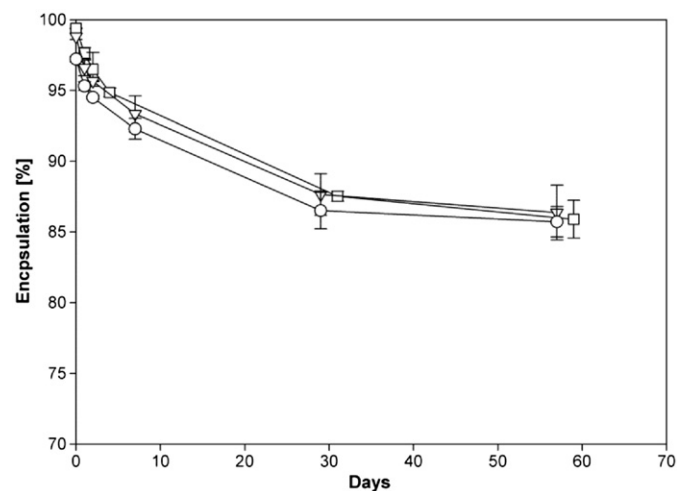
Fig. 8. Storage release of salt in duplex emulsions mixed in the high-shear mixer at 10,000 rpm for (□) 2 min, (▽) 5 min and (○) 10 min.

3.3.2. Cross-flow membrane emulsification

Duplex emulsions prepared with the cross-flow membrane were stored for up to 70 day, during which their conductivity was measured. Fig. 9 shows storage encapsulation for emulsions produced using the cross-flow membrane at various TMPs and the CFV of 0.11 m s^{-1} (Fig. 9a), 0.17 m s^{-1} (Fig. 9b) and 0.22 m s^{-1} (Fig. 9c). The data show that the release of salt over the storage period was higher for low TMPs and high CFVs. This trend is similar to the encapsulation measured immediately after emulsification (Fig. 6a). A possible explanation for this might be that at high CFVs and low TMPs, the emulsion droplets are smaller than those
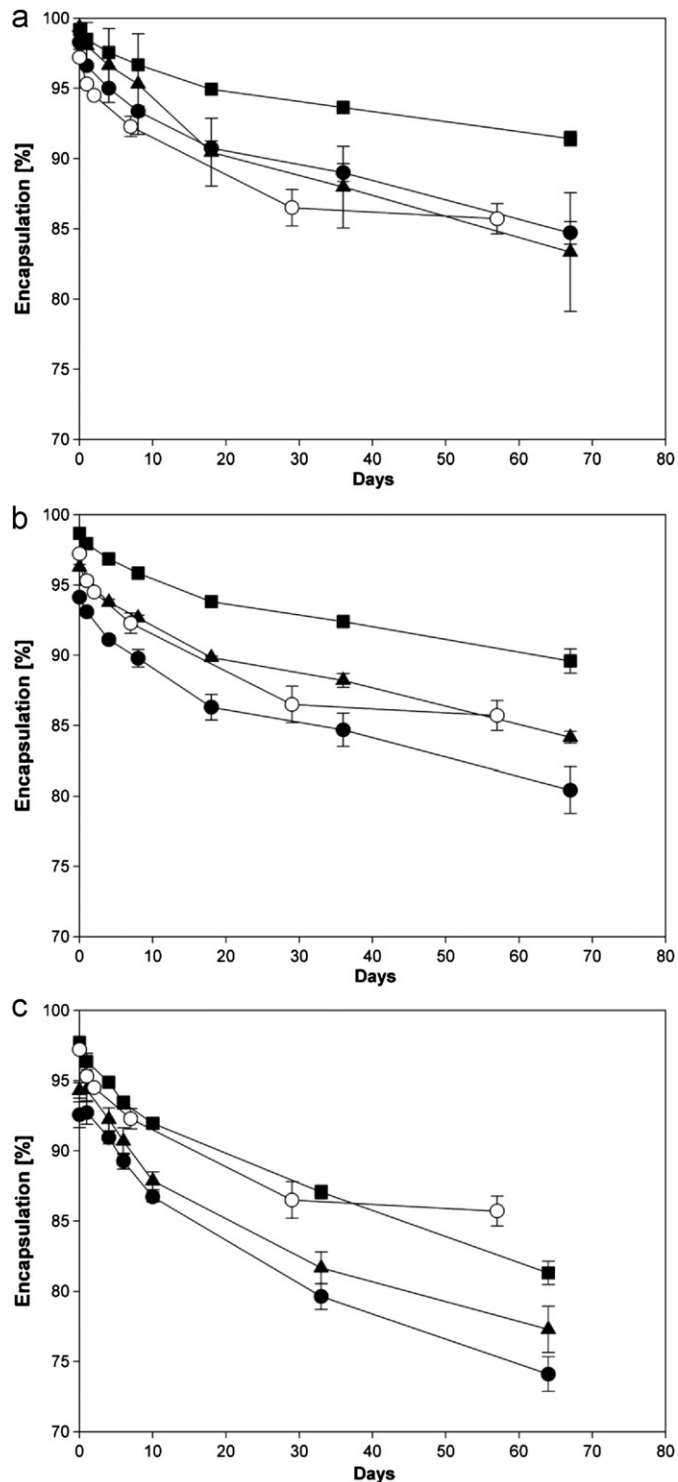
produced at lower CFVs and higher TMPs (Fig. 3). As a result, larger interfacial area is created, which facilitates molecular transport between the two water phases.

Fig. 9 also includes the storage encapsulation curve of emulsions prepared with the high-shear mixer. For the CFV of 0.11 and 0.17 m s^{-1}, the storage salt release in the Silverson-made emulsions is similar to emulsions made with the cross-flow membrane. However, salt release in emulsions prepared at the highest CFV (0.22 m s^{-1}) is somewhat higher than the release in emulsions made with the high-shear mixer. This is quite unexpected as membrane emulsification is commonly considered advantageous [6] for the production of shear-sensitive duplex emulsions.

3.3.3. Rotating membrane emulsification

Fig. 10 presents the data on the storage salt release from duplex emulsions made with the SPG rotating membrane at 40–100 kPa TMP and 300–1200 rpm rotating frequency. The encapsulation of salt in emulsions prepared with the high-shear mixer has also been plotted on the graphs, for reference. It can be seen that over the storage period, the release of salt differs significantly between emulsions prepared by the two methods. With no considerable influence of processing parameters (TMP and RV) on the salt release, all emulsions prepared with the rotating membrane showed better encapsulation of salt on storage (∼92%) than emulsions prepared with the high-shear mixer (∼87%).

Differences in performance between emulsions produced with the high-shear mixer, the cross-flow membrane and the rotating membrane are explained in terms of: (i) emulsion droplet size, and (ii) shear forces that duplex droplets were subjected to during emulsification. Table 3 summarises the data presented so far. It can be seen that droplet size of emulsions prepared with the high-shear mixer (∼14 μm) are comparable to the minimum droplet size obtained with the cross-flow membrane (average of ∼13 μm for 0.22 m s^{-1} CFV) and the rotating membrane (average of ∼11 μm for 1200 rpm RV).

Salt encapsulation measured directly after emulsification is highest for the rotating membrane (99.5–98.6%; a range that depends on the applied TMP and RV, Fig. 7). The encapsulation of emulsions made with the high-shear mixer is slightly lower (99.4–97.2%, Fig. 5), with the lowest salt encapsulation for emulsions made with the cross-flow membrane (99.3–92.5%, Fig. 6). As explained in Section 3.2.3, this is probably a consequence of the magnitude and duration of shear forces acting on duplex droplets during the emulsification process.

The percentage decrease in salt encapsulation during the storage period was also calculated. As seen from Table 3 the % loss of salt from the internal water phase is largest for the cross-flow membrane (between 7.8 and 19.9% depending on the applied CFV and TMP), followed by high-shear emulsification (12.6 ± 0.9%, an average of all mixing times), and lowest for the rotating membrane (7.9 ± 1.1%, an average of all emulsions).

Due to the fact that: (i) the minimum droplet size and droplet size distribution (data not shown) obtained by all emulsifying techniques are similar, and (ii) there is no visible difference in morphology of the internal water droplets (W_1) between the analysed samples; the interfacial area is unlikely to be the only factor causing markedly different encapsulation properties of these duplex emulsions. Therefore, the reason for this behaviour could be associated with the emulsification process and interfacial properties of the system. It was reported by Okochi and Nakano [17], that the release of a series of drugs from duplex $W_1/O/W_2$ emulsions was slower when emulsions were prepared by the membrane as compared to a stirring method. This was explained by surface properties of droplets, and a distinctively different way of emulsifier deposition and orientation at the interface in these two methods. Based on X-ray small angle scattering, it was established that during membrane emulsification surfactants adsorb at the interface in a homogenous manner. As a result, a densely packed layer of surfactant molecules with an isotropic orientation is created, which then is said to provide a mechanical barrier against molecular transport across the interface. This does not happen in the stirring process.

This hypothesis, however thermodynamically surprising, would correspond to our data on the storage salt release. In the case of cross-flow emulsification, a homogenous and dense layer of surfactant molecules forms at the interface during droplet formation at the tip of the membrane pore. However, subsequent intensive processing inside the membrane module and the gear pump disturbs the molecular orientation at the interface. This may lead to an irregular film of surfactants, and thus a weaker barrier for the migration of ions. In the high-shear mixer, due to a random deposition of surfactant molecules during emulsification, an anisotropic layer of surfactant is created. This "leaky" interface and similar droplet size for all emulsions prepared with this technique would lead to a comparable release of salt over the storage period. Finally, for the rotating membrane, mildness of the emulsification process ensures that the densely packed layer of surfactant is not further disturbed during batch emulsification, and thus the rate of salt release is slower than for emulsions made with the high-shear mixer and the cross-flow membrane. However, further work is required to investigate the suggested phenomenon.

From the perspective of industrial technology, SPG membrane emulsification has been reported [32] to have low dispersed phase fluxes. For the range of the applied TMPs in the cross-flow membrane, the obtained fluxes of the dispersed phase were between 8 and 111 L m^{-2} h^{-1}. With the rotating membrane however, fluxes up to 970 L m^{-2} h^{-1} (at 100 kPa TMP) could be achieved. For the

Fig. 9. Storage release of salt in duplex emulsions prepared using (○) the high-shear mixer at 10 min@10,000 rpm and cross-flow membrane at TMP of (●) 20 kPa, (▲) 40 kPa and (■) 80 kPa and CFV of (a) 0.11 m s^{-1}, (b) 0.17 m s^{-1}, (c) 0.22 m s^{-1}.
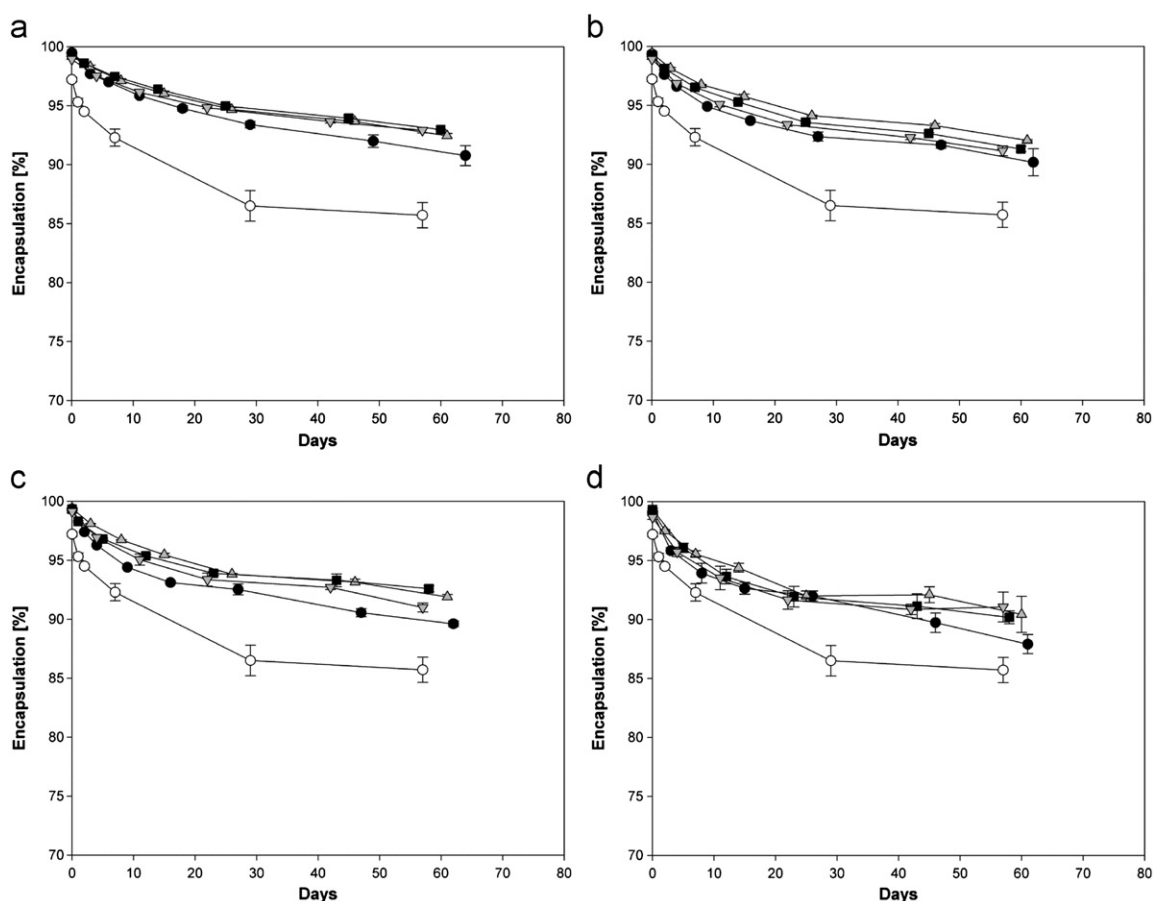
Fig. 10. Storage release of salt in duplex emulsions prepared using (○) the high-shear mixer at 10 min@10,000 rpm and rotating membrane at TMP of (●) 40 kPa, (▲) 60 kPa, (■) 80 kPa and (▼) 100 kPa and RV of (a) 300 rpm, (b) 600 rpm, (c) 900 rpm, (d) 1200 rpm.

Table 3
Summary of droplet size and encapsulation data for all processing techniques.

	High-shear mixer	Cross-flow membrane	Rotating membrane
Droplet size [µm]	13.6 ± 0.6	12.2–40**	8.5–40.3**
Salt encapsulation during emulsification [%]	99.4–97.2*	99.3–92.5**	99.5–98.6**
Loss of salt on storage [%]	12.6 ± 0.9	7.8–19.9**	7.9 ± 1.1

* Range of values reflects different encapsulation efficiency for emulsions mixed for 2, 5 and 10 min.
** Range of values reflects different encapsulation efficiency for emulsions produced at varied TMP, CFV and RV.

commercial production, amongst others, the lifespan of the membranes needs to be carefully considered. It will depend on the membrane resistance to fouling and the effective cleaning process, which is yet to be established (i.e., limitations of the heat treatment for the rotating membrane).

4. Conclusions

Three different techniques: high-shear mixer, cross-flow membrane and rotating membrane were used for the secondary emulsification step in the production of duplex $W_1/O/W_2$ emulsions. Droplet size and salt release from duplex emulsions were investigated.

Droplet size of emulsions produced with both membrane techniques was shown to decrease with the drag force generated by either CFV or RV. For example, in cross-flow emulsification at 40 kPa TMP droplets are ~35 µm for 0.11 m s^{-1}, ~16 µm for 0.17 m s^{-1} and ~13 µm for 0.22 m s^{-1} CFV. It was also shown that droplet size increased with the applied TMP; e.g., duplex emulsions produced with the rotating membrane at 40 kPa TMP have droplet sizes of ~20 µm, which increased to ~30 µm at

60 kPa, to ~35 µm at 80 kPa and finally to ~40 µm at 100 kPa (data for 300 rpm RV). Since a similar minimum droplet size (~12 µm) was obtained by all three emulsifying techniques, it is suggested that at the highest shear forces generated in each emulsification technique, the droplet sizes are primarily determined by the rate of the interfacial tension decrease.

Salt release from the internal water phase of duplex emulsions varies between the three emulsifying techniques used. The slowest release rate was observed when duplex emulsions were made with the rotating membrane (7.9 ± 1.1% loss of salt on storage), followed by high-shear emulsification (12.6 ± 0.9%) and the highest release for the cross-flow membrane (7.8–19.9%). These differences were explained in terms of (i) emulsion droplet size, thus the interfacial area available for molecular transport, and (ii) the effect of shear forces applied in each emulsification process and thus different interfacial properties of adsorbed surfactants.

It is proposed that during droplet formation in both membrane techniques, a homogenous deposition of surfactant molecules at the interface results in a dense and isotropic layer of surfactant. This layer is likely to provide a better mechanical barrier against

ionic diffusion between the two water phases of duplex emulsions, thus resulting in slower salt release. However, during cross-flow emulsification, shear forces generated in the membrane system disturb the homogenously packed surfactant molecules, creating a "leaky" interface.

Acknowledgements

Reference

[1] U. Lesmes, D.J. McClements, Structure-function relationships to guide rational design and fabrication of particulate food delivery systems, Trends Food Sci. Technol. 20 (10) (2009) 448–457.

[2] R. Mezzenga, Equilibrium and non-equilibrium structures in complex food systems, Food Hydrocolloids 21 (2007) 674–682.

[3] David Julian McClements, Food Emulsions-Principles, Practices, and Techniques, CRC Press, Boca Raton, 2005.

[4] E. Dickinson, M. Akhtar, Water-in-oil-in-water multiple emulsions stabilized by polymeric and natural emulsifiers, in: E. Dickinson, R. Miller (Eds.), Food Hydrocolloids, Fundamentals of Formulation, The Royal Society of Chemistry, Cambridge, 2001, pp. 133–144.

[5] V. Schadler, E.J. Windhab, Continuous membrane emulsification by using a membrane system with controlled pore distance, Desalination 189 (2006) 130–135.

[6] C. Charcosset, I. Limayem, H. Fessi, The membrane emulsification process—a review, J. Chem. Technol. Biotechnol. 79 (2004) 209–218.

[7] S.J. Peng, R.A. Williams, Controlled production of emulsions using a crossflow membrane: Part I: Droplet formation from a single pore, Chem. Eng. Res. Des. 76 (1998) 894–901.

[8] S.M. Joscelyne, G. Trägårdh, Membrane emulsification—a literature review, J. Membr. Sci. 169 (2000) 107–117.

[9] C.J. Cheng, L.Y. Chu, R. Xie, X.W. Wang, Hydrophobic modification and regeneration of Shirasu Porous glass membranes on membrane emulsification performance, Chem. Eng. Technol. 31 (2008) 377–383.

[10] A. Aserin, Multiple emulsions, Technology and Applications, John Wiley & Sons, Inc., 2008.

[11] G.T. Vladisavljević, H. Schubert, Influence of process parameters on droplet size distribution in SPG membrane emulsification and stability of prepared emulsion droplets, J. Membr. Sci. 225 (2003) 15–23.

[12] Y. Mine, M. Shimizu, T. Nakashima, Preparation and stabilization of simple and multiple emulsions using a microporous glass membrane, Colloids Surf., B 6 (1996) 261–268.

[13] G.T. Vladisavljević, M. Shimizu, T. Nakashima, Production of multiple emulsions for drug delivery systems by repeated SPG membrane homogenization: influence of mean pore size, interfacial tension and continuous phase viscosity, J. Membr. Sci. 284 (2006) 373–383.

[14] G.T. Vladisavljević, M. Shimizu, T. Nakashima, Preparation of monodisperse multiple emulsions at high production rates by multi-stage premix membrane emulsification, J. Membr. Sci. 244 (2004) 97–106.

[15] I. Scherze, R. Knöfel, G. Muschiolik, Automated image analysis as a control tool for multiple emulsions, Food Hydrocolloids 19 (2005) 617–624.

[16] S. van der Graaf, C.G.P.H. Schroën, R.M. Boom, Preparation of double emulsions by membrane emulsification—a review, J. Membr. Sci. 251 (2005) 7–15.

[17] H. Okochi, M. Nakano, Comparative study of two preparation methods of w/o/w emulsions: stirring and membrane emulsification, Chem. Pharm. Bull. 45 (1997) 1323–1326.

[18] N. Aryanti, R.A. Williams, R. Hou, G.T. Vladisavljević, Performance of rotating membrane emulsification for o/w production, Desalination 200 (2006) 572–574.

[19] Q. Yuan, N. Aryanti, R. Hou, R.A. Williams, Performance of slotted pores in particle manufacture using rotating membrane emulsification, Particuology 7 (2009) 114–120.

[20] K. Pays, J. Giermanska-Kahn, B. Pouligny, J. Bibette, F. Leal-Calderon, Double emulsions: how does release occur? J. Controlled Release 79 (2002) 193–205.

[21] A. Pawlik, P.W. Cox, I.T. Norton, Food grade duplex emulsions designed and stabilised with different osmotic pressures, J. Colloid Interface Sci. 352 (2010) 59–67.

[22] T. Nakashima, M. Shimizu, M. Kukizaki, Membrane Emulsification Operation Manual, Industrial Research Institute of Miyazaki Prefecture, Japan, 1991.

[23] A.T. Utomo, M. Baker, A.W. Pacek, Flow pattern, periodicity and energy dissipation in a batch rotor-stator mixer, Chem. Eng. Res. Des. 86 (2008) 1397–1409.

[24] D.J. McClements, Food Emulsions, Principles, Practices and Techniques, CRS Press, 2005.

[25] R.E. Meredith, C.W. Tobias, Conductivities in emulsions, J. Electrochem. Soc. 108 (1960) 286–290.

[26] S.J. Peng, R.A. Williams, Controlled production of emulsions using a crossflow membrane: Part I: Droplet formation from a single pore, Chem. Eng. Res. Des. 76 (1998) 894–901.

[27] A. Timgren, G. Trägårdh, C. Trägårdh, A model for drop size prediction during cross-flow emulsification, Chem. Eng. Res. Des. 88 (2010) 229–238.

[28] V. Schröder, O. Behrend, H. Schubert, Effect of dynamic interfacial tension on the emulsification process using microporous, ceramic membranes, J. Colloid Interface Sci. 202 (1998) 334–340.

[29] E. Egidi, G. Gasparini, R.G. Holdich, G.T. Vladisavljević, S.R. Kosvintsev, Membrane emulsification using membranes of regular pore spacing: droplet size and uniformity in the presence of surface shear, J. Membr. Sci. 323 (2008) 414–420.

[30] C. Charcosset, Preparation of emulsions and particles by membrane emulsification for the food processing industry, J. Food Eng. 92 (2009) 241–249.

[31] E. Lepercq-Bost, M.L. Giorgi, A. Isambert, C. Arnaud, Use of the capillary number for the prediction of droplet size in membrane emulsification, J. Membr. Sci. 314 (2008) 76–89.

[32] A.J. Abrahamse, R. van Lierop, R.G.M. van der Sman, A. van der Padt, R.M. Boom, Analysis of droplet formation and interactions during cross-flow membrane emulsification, J. Membr. Sci. 204 (2002) 125–137.

[33] N.C. Christov, D.N. Ganchev, N.D. Vassileva, N.D. Denkov, K.D. Danov, P.A. Kralchevsky, Capillary mechanisms in membrane emulsification: oil-in-water emulsions stabilized by Tween 20 and milk proteins, Colloids Surf., A 209 (2002) 83–104.

[34] G.T. Vladisavljević, T. Nakashima, M. Shimizu, H. Schubert, M. Nakajima, Production of monodispersed emulsions using Shirasu porous glass membranes, in: A.M. Spasic, J.P. Hsu (Eds.), Finely Dispersed Particles. Micro-, Nano-, and Atto-Engineering, CRC Press, Taylor & Francis Group, 2006, pp. 396–429.

[35] M. Bonnet, M. Cansell, A. Berkaoui, M.H. Ropers, M. Anton, F. Leal-Calderon, Release rate profiles of magnesium from multiple W/O/W emulsions, Food Hydrocolloids 23 (2009) 92–101.